Science Advances
AAAS

advances.sciencemag.org/cgi/content/full/5/5/eaaw2205/DC1

Supplementary Materials for

Scalable electrochromic nanopixels using plasmonics

Jialong Peng, Hyeon-Ho Jeong, Qianqi Lin, Sean Cormier, Hsin-Ling Liang, Michael F. L. De Volder, Silvia Vignolini, Jeremy J. Baumberg*

*Corresponding author. Email: jjb12@cam.ac.uk

Published 10 May 2019, *Sci. Adv.* **5**, eaaw2205 (2019)
DOI: 10.1126/sciadv.aaw2205

The PDF file includes:

Other Supplementary Material for this manuscript includes the following:

(available at advances.sciencemag.org/cgi/content/full/5/5/eaaw2205/DC1)

Movie S1 (.mov format). Matrix (6 × 6) of the DF scattering images of the *e*NPoMs as a function of time during CV cycle in the range of –0.2 to 0.6 V (versus Ag/AgCl) with a scan rate of 50 mV/s.
Movie S2 (.mov format). DF scattering images of four different particles (in row) of four different *e*NPoMs composed of 11-, 13-, 18-, and 20-nm PANI thicknesses as a function of time during CV cycle in the range of –0.2 to 0.6 V (versus Ag/AgCl) with a scan rate of 50 mV/s.
Movie S3 (.mov format). DF scattering images of the *e*NPoM metasurfaces as a function of time during CV cycle in the range of –0.2 to 0.6 V (versus Ag/AgCl) with a scan rate of 50 mV/s.

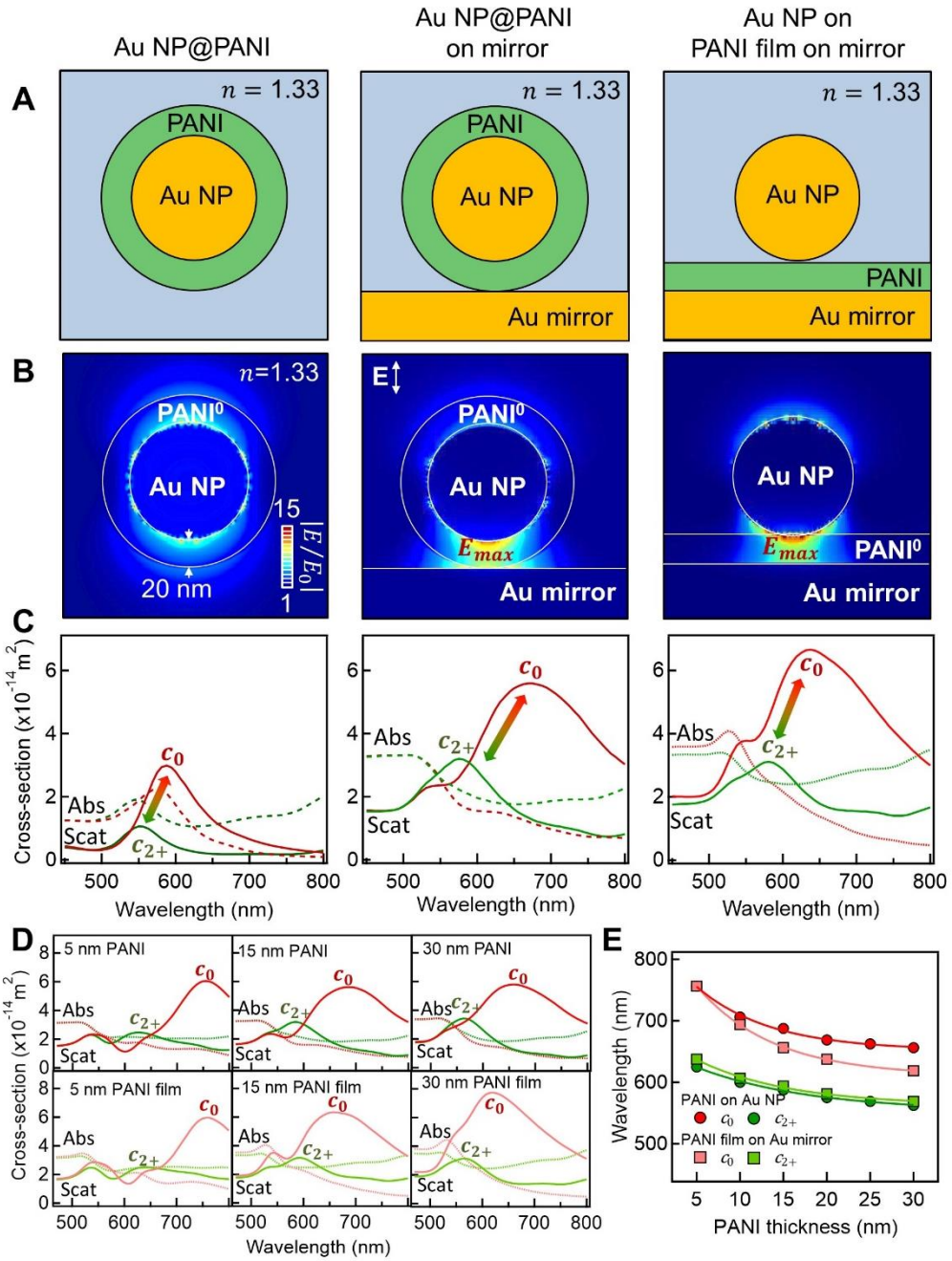

Fig. S1. FDTD simulations of Au NPs and *e*NPoMs. (**A**) Schematics and (**B**) optical near-field enhancements of Au NPs coated with a 20nm PANI shell layer (left panel) and two different *e*NPoM geometries (middle: PANI shell surrounding Au NP, right: PANI layer only on Au mirror). (**C**) Corresponding simulated optical scattering (solid lines) and absorption spectra (dotted lines) with reduced (red) and oxidized (green) PANI. (**D**) Simulated optical scattering (solid lines) and absorption spectra (dotted lines) of the two *e*NPoMs *vs* wavelength for different PANI thicknesses (5 nm to 30 nm from left to right). (**E**) Corresponding coupled plasmon mode peaks as a function of PANI thickness.

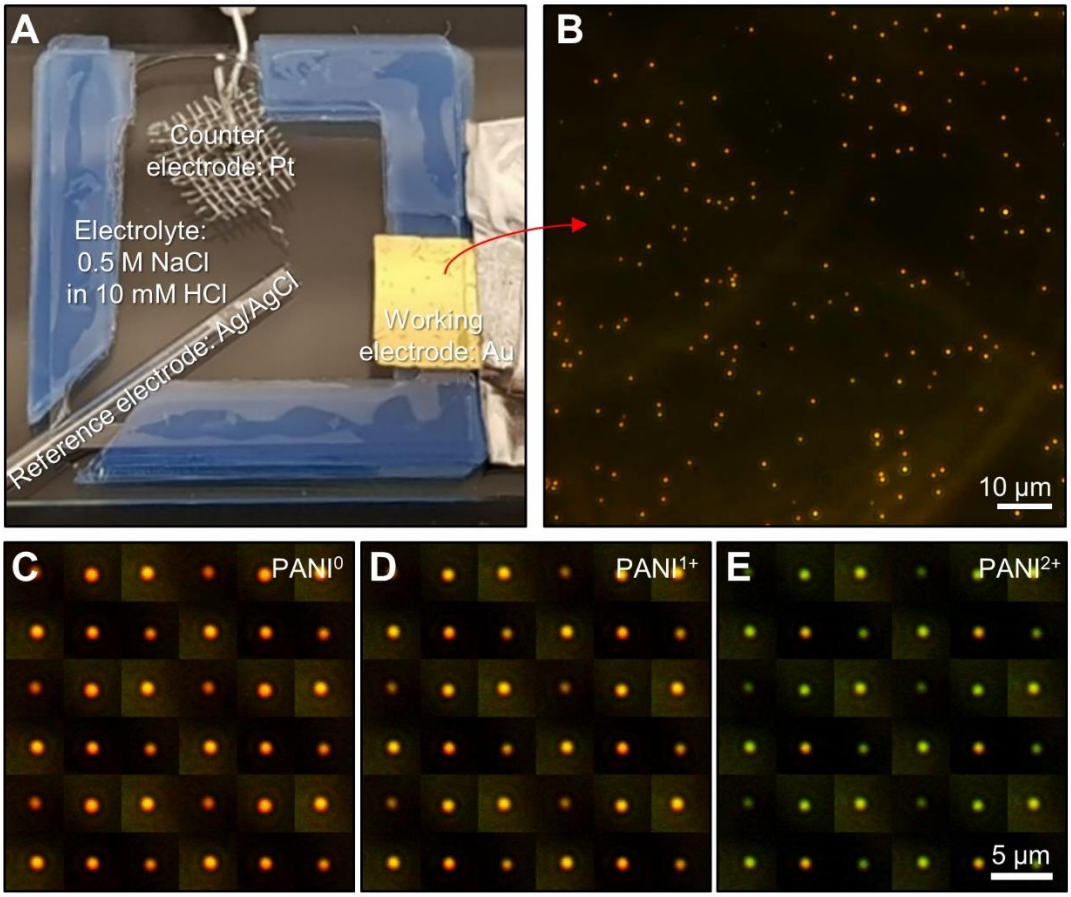

Fig. S2. Electrochemical cell. (**A**) Image of electrochemical cell with *e*NPoMs on mirror layer also used as working electrode. Photo credit: J. Peng & H.-H. Jeong, University of Cambridge. (**B**) Large-area DF scattering image of sparse *e*NPoMs. DF scattering images of *e*NPoMs at (**C**) $PANI^{0}$ (full reduction), (**D**), $PANI^{1+}$ (half oxidation), and (**E**) $PANI^{2+}$ (full oxidation).

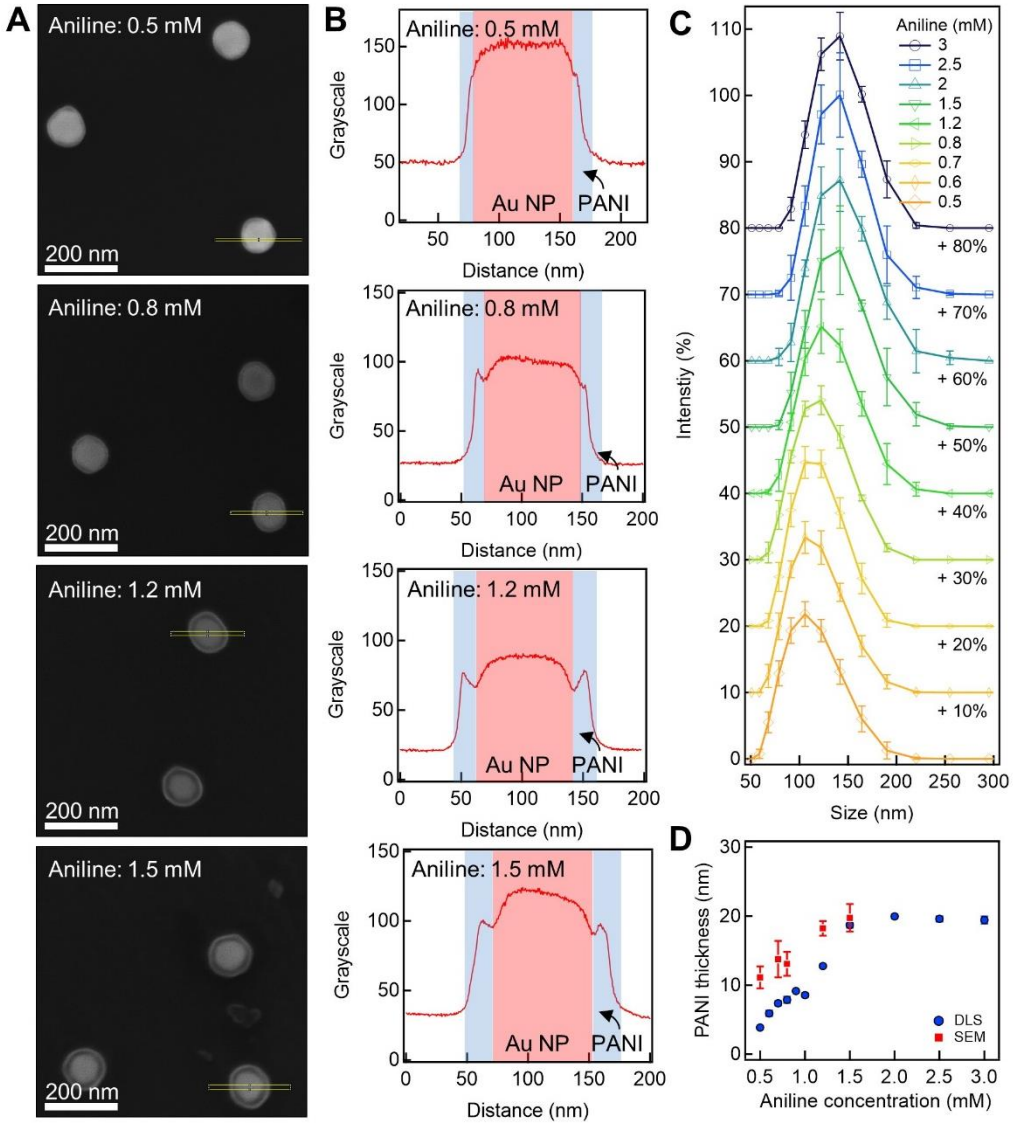

Fig. S3. PANI coating on Au NPs with thickness control. (**A**) Scanning electron microscope (SEM) images of 80 nm Au NPs coated with different PANI thickness. (**B**) Corresponding cross-sections and (**C**) dynamic light scattering (DLS) spectra, showing increasing hydrodynamic diameter of the NPs for increasing monomer concentration in the coating process. (**D**) PANI thickness measured by SEM (red squares) and DLS (blue circles) as a function of aniline monomer concentration.

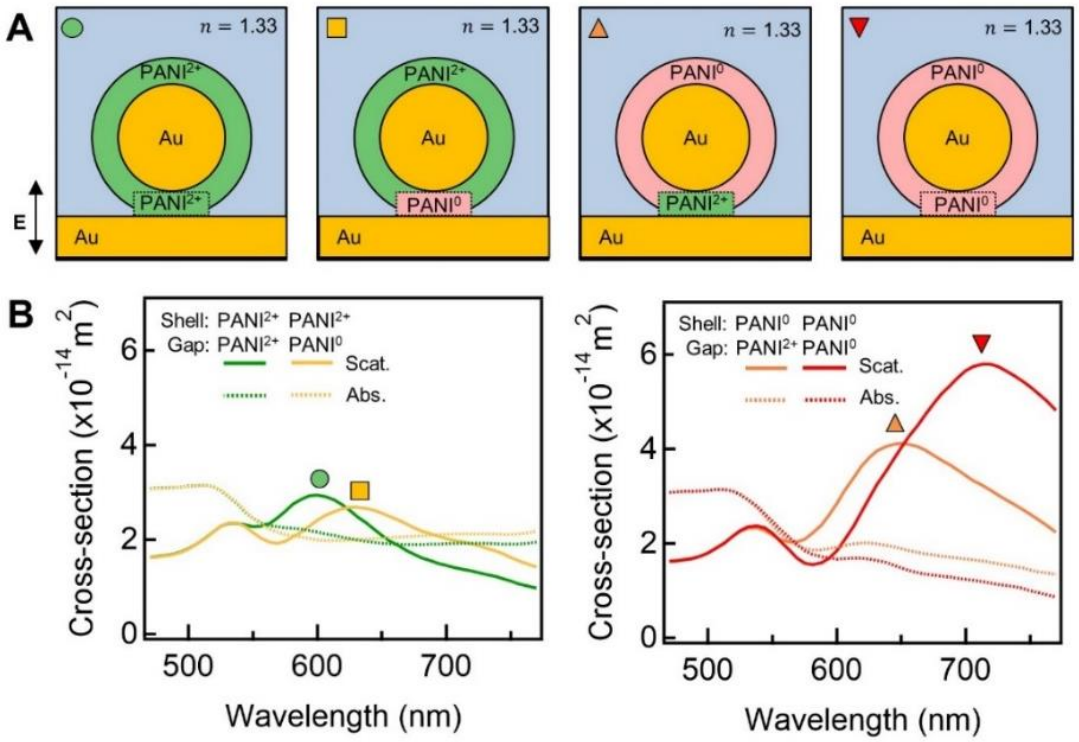

Fig. S4. FDTD numerical simulation of *e*NPoM for different redox states in the gap. (**A**) Schematic NPoMs for different situations of redox within the PANI shell (green circle: $PANI^{2+}$ shell with $PANI^{2+}$ gap, yellow square: $PANI^{2+}$ shell with $PANI^{0}$ gap, orange upper triangle: $PANI^{0}$ shell with $PANI^{2+}$ gap, red lower triangle: $PANI^{0}$ shell with $PANI^{0}$ gap). (**B**) Corresponding scattering (solid line) and absorption spectra (dotted line) *vs* wavelength. Partial changes in the PANI redox switching through the shell volume will lead to smaller changes in the effective refractive index surrounding the nanoparticle, so reducing the corresponding color dynamic range.

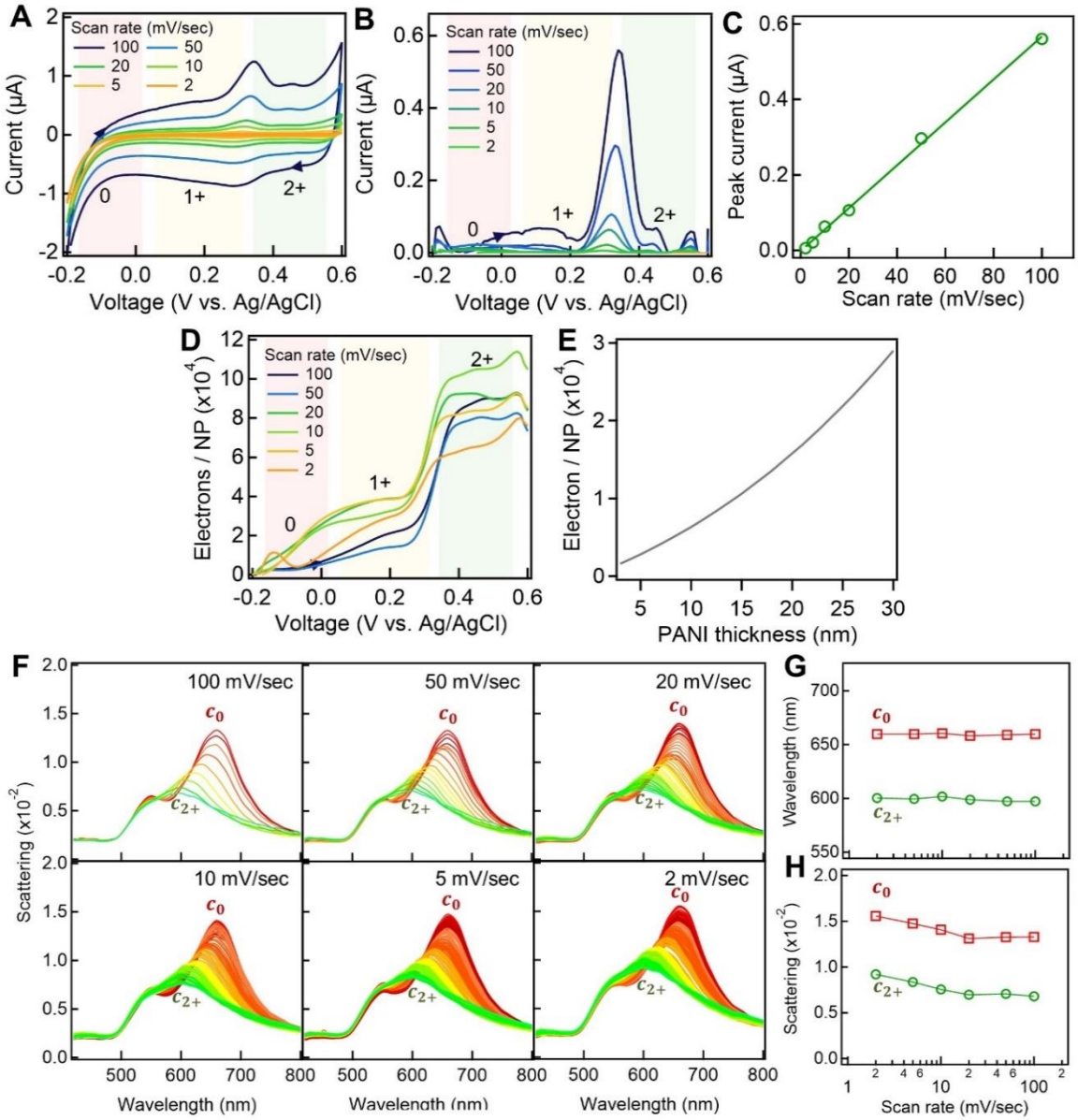

Fig. S5. Electrochemical analysis of *e*NPoMs. (**A**) CV curves of *e*NPoMs *vs* scan rate from 2 to 100 mV/sec, and (**B**) after background correction. (**C**) Peak current in CV *vs* scan rate from 2 to 100 mV/sec. (**D**) Charge transferred via the gap *vs* applied potential. (**E**) Estimated electron transfer per *e*NPoM *vs* PANI thickness. Molecular weight and density of PANI are 0.3 mg/mol and 1.25 g/mL (*34*). (**F**) DF scattering spectra of a single *e*NPoM for different scan rates shown, and (**G**) their corresponding peak wavelengths and (**H**) intensities as a function of scan rate.

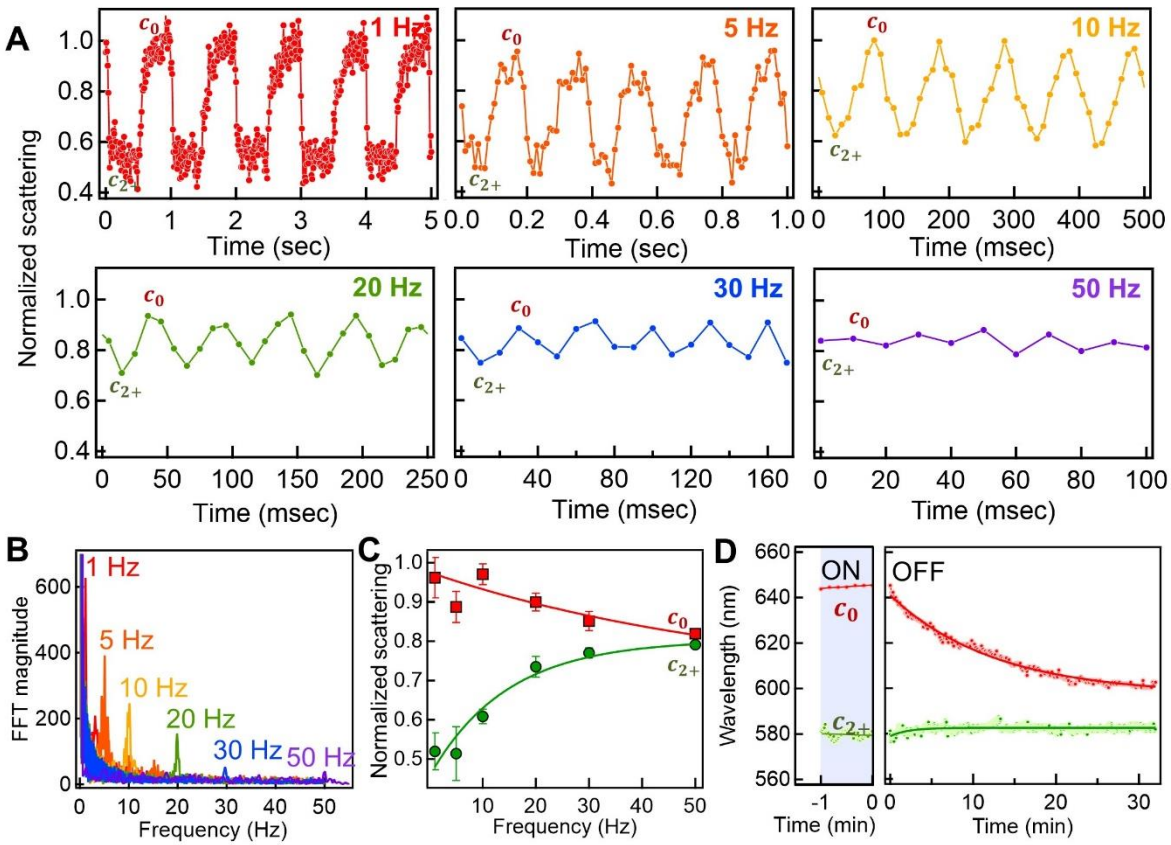

Fig. S6. Reversible optical switching of *e*NPoMs. (**A**) DF scattering intensities of an *e*NPoM at the peak wavelength c_0 in response to square waves at 1 (red), 5 (orange), 10 (yellow), 20 (green), 30 (blue), and 50 Hz (violet). (**B**) Corresponding FFT analysis and (**C**) optical contrast *vs* frequency. (**D**) Retention of *e*NPoM redox state. Left panel shows wavelength positions of c_0 and c_{2+} for the *e*NPoM at -0.2 and 0.6 V. Right panel shows corresponding peak shifts after switching off the external potential.

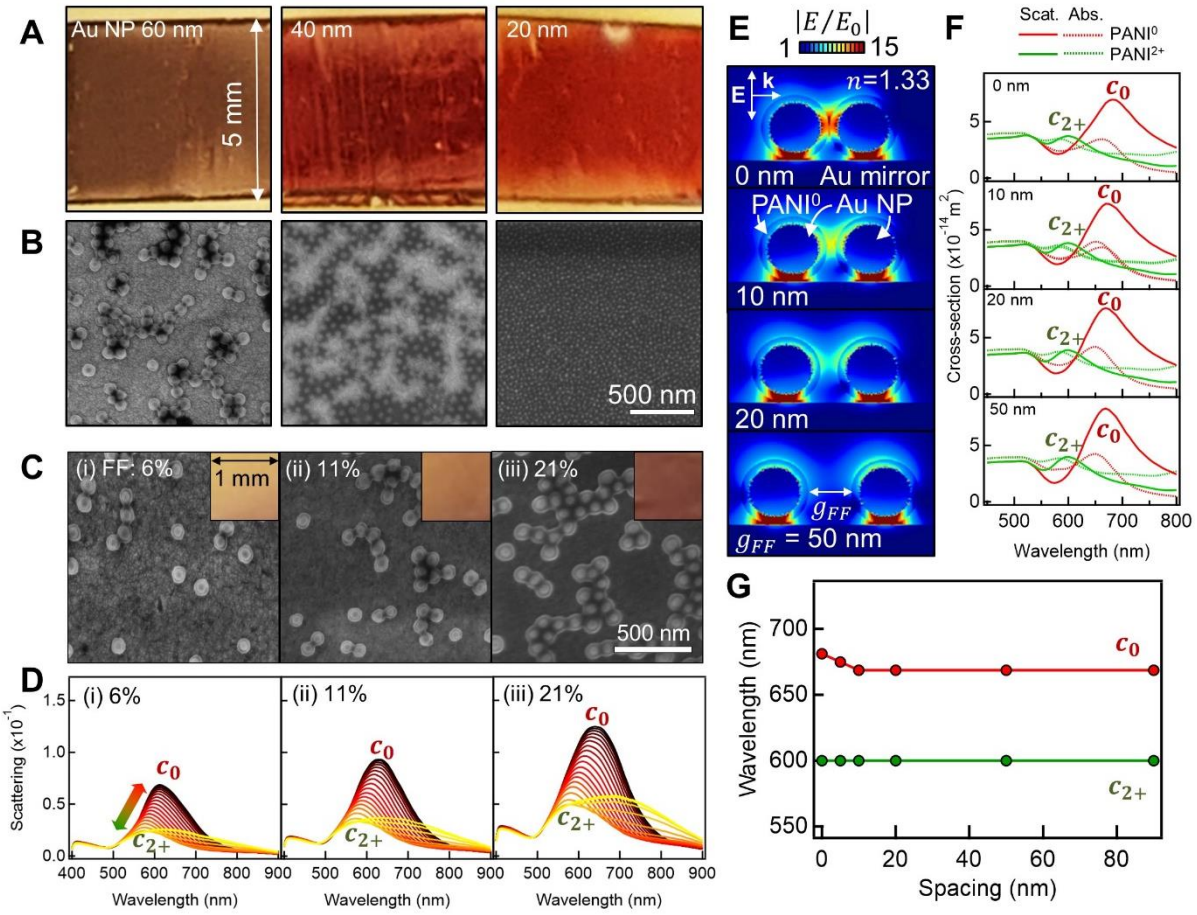

Fig. S7. *e*NPoM metasurfaces. (**A**) Images of *e*NPoM metasurfaces composed of 60, 40, and 20 nm Au NPs (from left to right) (Photo credit: J. Peng & H.-H. Jeong, University of Cambridge) and (**B**) their corresponding SEM images. (**C**) SEM images of the eNPoM metasurfaces composed of 60 nm Au NPs with different fill fraction from 6 to 21% (from left to right) and (**D**) their corresponding DF scattering spectra *vs* voltage applied from -0.3 ↔ 0.8 V. (**E**) Optical near-field enhancements of two *e*NPoM *vs* lateral separation. (**F**) Corresponding simulated optical scattering (solid lines) and absorption spectra (dotted lines) with reduced (red) and oxidized (green) PANI. (**G**) Corresponding coupled plasmon mode peaks *vs* lateral separation.

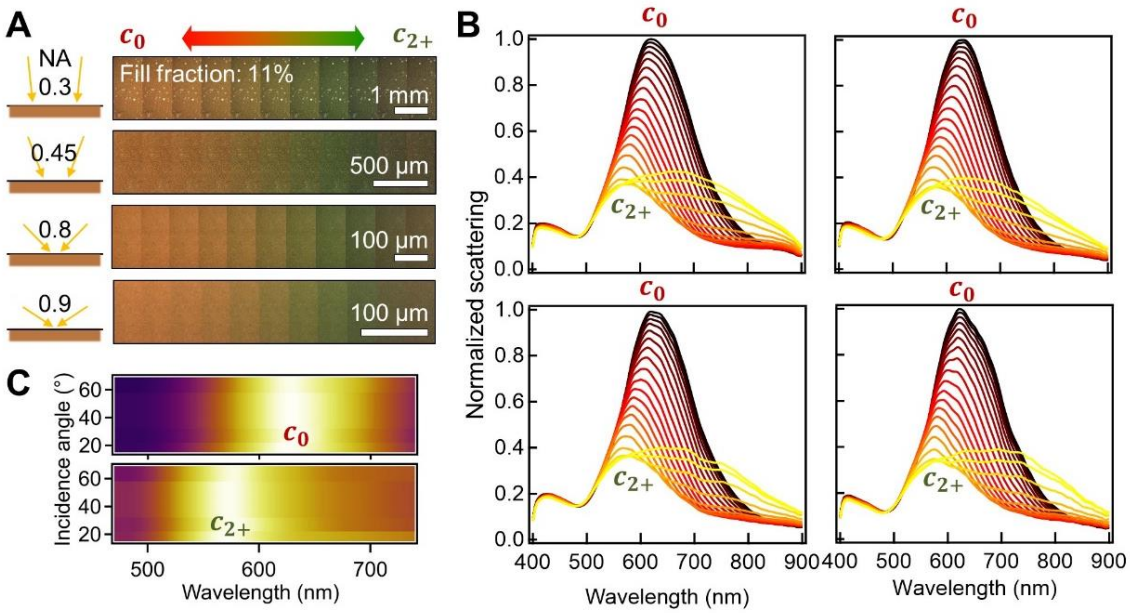

Fig. S8. Angular dependence of *e*NPoM metasurfaces. (**A**) DF images of the *e*NPoM metasurfaces at numerical apertures of 0.3, 0.45, 0.8, and 0.9 *vs* voltage applied from -0.3 ↔ 0.8 V. (**B**) Corresponding DF scattering spectra, and (**C**) 2D maps (top: c_{2+}, bottom: c_0) *vs* incident angle of the light.

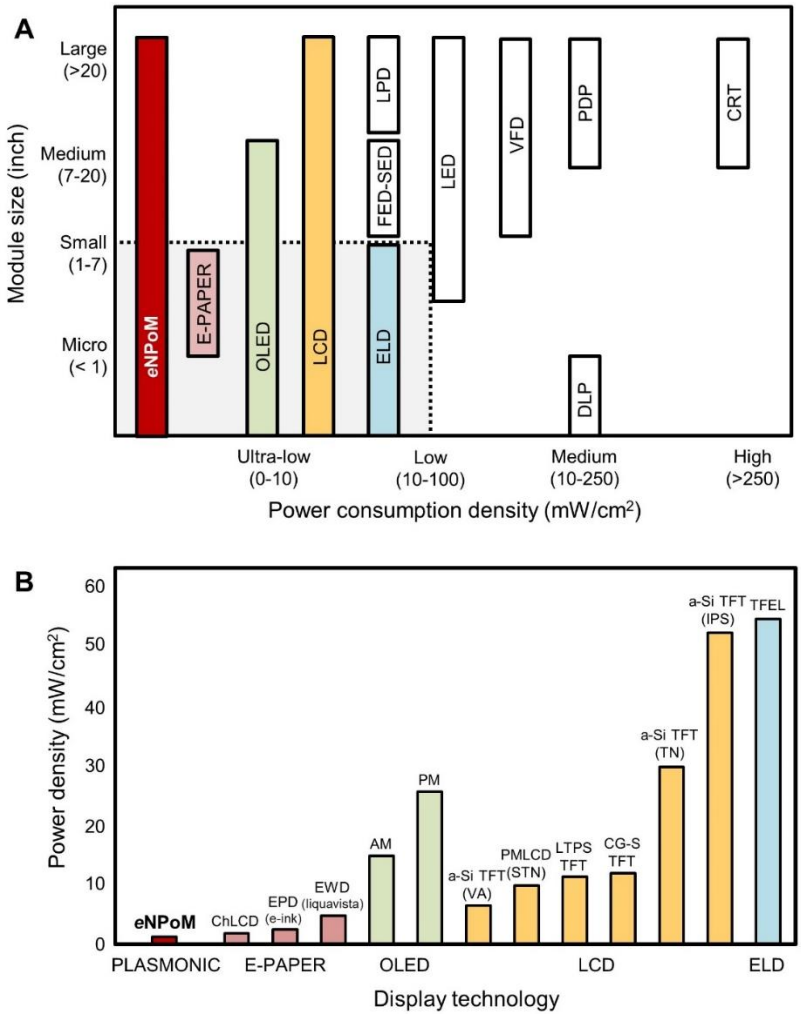

Fig. S9. Power density of various displays (*35*). (**A**) Comparison of displays against module size and power consumption. (**B**) Power density of displays. Electronic paper (E-PAPER): electrophoretic display (EPD), electro-wetting display (EWD), cholesteric LCD (ChLCD), organic light-emitting display (OLED): passive matrix (PM), active matrix (AM), liquid crystal display (LCD): amorphous silicon (a-Si), continuous grain silicon (CGS), low temperature polycrystalline silicon (LTPS), twisted nematic (TN), super TN (STN), vertical alignment (VA), in-plane switching (IPS), thin film transistor (TFT), electroluminescent display (ELD): thin film electroluminescent (TFEL), field emission display (FED), surface-conduction electron-emitter display (SED), laser phosphor display (LPD), light-emitting diode (LED), vacuum fluorescent display (VFD), digital light processing (DLP), plasma display panel (PDP), cathode ray tube (CRT).

Table S1. Comparison of electrochromic plasmonic reflective devices.

Type	Color gener-ation	Color Switching	Single unit area (nm^2)	Switch time (ms)	Long-term stability	Method	Ref
*e*NPoM metasurfaces	Single Pixel	Dynamic (578 nm – 642 nm)	~11310	30	>3 months	Self-assembly (solution process)	This study
Nano-slits + conductive polymers			~57600	< 10		FIB, sputtering	(*12*)
MINs with conductive polymers	RGB combi-nations	On-off	>102400	200 - 1000	unreported	Self-assembly, ALD, evaporation	(*10*, *11*)
Al MIMs with LC			~90000	~30		NIL (with EBL), evaporation, LC coating	(*9*)

*nanoimprint lithography (NIL), e-beam lithography (EBL), atomic layer deposition (ALD), polypyrrole (PPy), focused ion beam (FIB), liquid crystal (LC), metal-insulator-metal (MIM), metal−insulator−nanohole (MIN).

Supplementary Information

Estimate of charge transferred per cycle:

The volume of the PANI shell (thickness t) per NP (diameter D) is given by

$$V_{PANI} = \frac{4}{3}\pi\left[\left(\frac{D}{2}+t\right)^3 - \left(\frac{D}{2}\right)^3\right]$$

which given the density of PANI ρ=1.25 g/cm^3 and molecular weight of each unit M_w=0.3 mg/mol implies 2x10^4 electrons per NP are needed for each individual redox step. This compares with 3x10^4 electrons found from the experimental CV data.